WORLD CONFERENCE ON TIMBER ENGINEERING 2025
BRISBANE, AUSTRALIA
Advancing Timber for the Future Built Environment

EXPERIMENTAL DETERMINATION OF THE COMBINED LOADING BEHAVIOUR OF SCALED TIMBER FRAME WALLS SUBJECTED TO BENDING AND SHEAR

Dries Byloos[1†], Tine Engelen[1], Bram Vandoren[1]

ABSTRACT: The shift towards using more and higher timber structures comes with more questions regarding their structural behaviour. For instance, structural robustness and racking resistance are two important themes currently being researched more thoroughly. Within the context of structural robustness, timber walls could become self-supporting due to damage occurring to the underlying supporting elements. In such a scenario, timber walls are subjected to in-plane bending and possibly horizontal (shear) loads, a combination of load cases for which little knowledge has been developed in the context of timber frame construction. Therefore, an experimental and numerical campaign is presented in which six timber frame walls were tested. Two walls were loaded solely under in-plane horizontal loads until failure, and four walls were subjected to a combination of in-plane vertical (bending) and horizontal loads. Results showed that increasing the vertical loading lowered the horizontal load (or racking) resistance of the timber frame wall. The interaction behavior was also visible in the load-displacement diagram, which depicted a faster decrease in stiffness in the elastoplastic and plastic area of the wall and decreased yielding force whenever more vertical loading was applied. This interaction behavior was similar to the predictions according to mesoscale finite element models.

KEYWORDS: Combined loading, Timber Frame diaphragms, In-plane bending, Experimental, Numerical

1 – INTRODUCTION

The growing recognition of climate change has heightened the demand for sustainable building materials and practices to reduce carbon emissions in construction. Timber has emerged as a preferred alternative to conventional materials such as concrete and steel, sparking interest in developing timber frame structures [11, 14, 16]. Among the key research areas is the evaluation of structural robustness, assessing a structure's ability to withstand unforeseen loads without progressive collapse [13].

Studies on the robustness of timber frame structures focus on several aspects. For instance, robust design often parallels seismic design, emphasizing redundancy and ductility through features like metal connectors [1, 7]. Voulpiotis et al. [20, 21] developed methods for quantifying robustness and highlighted design adaptations for tall timber buildings. The updated Eurocode 5 (prEN 1995-1-1:2023) [4] recommends strategies such as alternative load paths and structural segmentation to enhance robustness. Nevertheless, further research is essential to advance robust design practices for timber-framed buildings as stated in [3, 9].

An important challenge in this context is understanding the load-bearing capacities of timber frame diaphragms under combined loading scenarios. For example, localized failures may induce in-plane bending in wall diaphragms, potentially reducing the overall load-bearing capacity. Limited existing studies have primarily focused on timber frame diaphragms under in-plane bending scenarios [17]. Research on racking resistance addressing lateral loads from wind or seismic activity has explored more factors such as openings, connectors, and sheathing materials [2, 10, 15]. However, these studies largely neglect scenarios involving simultaneous vertical and lateral loads, which may further reduce racking capacity in diaphragms positioned over large spans or openings, as illustrated in Figure 1. Current provisions in Eurocode 5 [5] address interaction behavior for individual timber elements but lack guidance on composite elements like wall diaphragms, leaving the effects of combined loading underexplored.

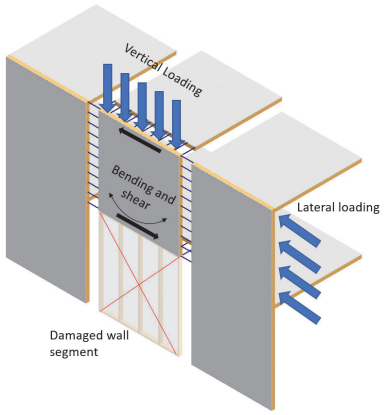

Figure 1: Simplified view of a diaphragm acting in possible combined loading.

[1]†Construction Engineering Research Group, Faculty of Engineering Technology, Hasselt University, Belgium, dries.byloos@uhasselt.be

https://doi.org/10.52202/080513-0371

A potential approach to determine this behavior involves using mathematical models, as outlined in [12, 19], or more advanced mesoscale numerical models, as described in [10]. However, these models primarily address the racking resistance of standard scenarios. Therefore, this research includes an experimental campaign in which two walls are tested under lateral loading, and four walls are tested under combined lateral and vertical (bending) loading. Secondly, a mesoscale finite element model based on the connection behavior is employed to simulate and compare results with the experimentally tested walls.

2 – MATERIALS AND METHODS

This Materials and Methods section outlines the general dimensions of the tested wall diaphragms, the experimental setup, and the numerical method used for the simulations.

2.1 WALL DIAPHRAGMS

The scaled timber frame diaphragms were constructed according to Figure 2. Each wall comprises C24 softwood studs and rails with 45 mm × 95 mm cross-sections. The rails are 3420 mm long, and the studs are 1110 mm high, resulting in a total wall height of 1200 mm. Seven studs, spaced 570 mm apart, are each connected to the rails using three nails (2.8 mm diameter, 80 mm length).

The walls are sheathed with 12.5 mm oriented strand board (OSB) panels on both framing sides. The OSB panels have mechanical properties of 9.4 N/mm² for the tensile strength, a modulus of elasticity of 3500 N/mm², and a shear modulus that equals 1080 N/mm². Screws were used as the sheathing-to-framing connections (5 mm diameter, 80 mm length). The connections were spaced 150 mm apart along both the rails and studs. The screws were predrilled using a 3 mm drill. Due to the relatively thin studs and using two rows of connectors, the intermediate and end distances do not meet the minimum requirements specified in EN 1995:1:1:2005 clause 8.7 [5].

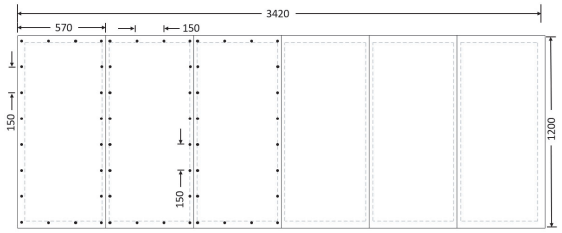

Figure 2: Technical drawing of the wall configuration. Dimensions in mm.

2.2 EXPERIMENTAL SETUP

The test setup for both the horizontal (shear) loading and the combined loading (shear and bending) experiments was largely similar, with the primary difference being the vertical loading points introduced in the combined loading experiments at the top of the specimen. Figure 3 illustrates the constructed test configuration, highlighting key components.

To maintain in-plane behavior during horizontal loading, four ball rollers were installed at the upper rail of the wall, with two placed on each side of the specimen. These rollers facilitated free movement with minimal friction while ensuring the wall remained in the intended plane. Steel U-profiles with smooth plywood plates were employed on the lower rail to mitigate the risk of lateral torsional buckling of the wall. The monotonic horizontal load was applied via a hydraulic cylinder. This cylinder was connected to a headpiece, which was, in turn, attached to the upper rail. The headpiece functioned to evenly distribute the applied horizontal load, thereby minimizing stress concentrations at the loading point and reducing the likelihood of splitting in the upper rail. To restrict the horizontal displacement of the lower rail, an L-shaped steel block was positioned at the opposite end of the applied load.

As the experiment analyzed a fully anchored wall, a tie-down system was required to mitigate potential uplift at the leading stud. Instead of a conventional tie-down, which would have restricted horizontal translation at the support point, two steel cables were positioned on each side of the leading stud. These cables were anchored to steel profiles, which were secured to the concrete reaction floor, and were pre-tensioned using a spanner to function as a rigid tie-down alternative. Finally, vertical loading was applied using four steel cables, with two cables positioned on each side of the wall per loading point. The amount of loading is shown in Table 1. These cables were anchored to the concrete reaction floor and were simultaneously tensioned until the desired downward force was achieved, as measured by a load cell at each loading point. The horizontal displacement was measured with an LVDT attached to the upper rail, and the vertical displacement was measured with LVDTs underneath each respective stud. The yield point of the specimens was evaluated using the equivalent energy elastoplastic method, following the same method applied in [17].

Table 1: Abbreviations of the different specimens and the applied total vertical loading.

ID	Total Vertical preload (kN)
S-1	0
S-2	0
C-1	8
C-2	12
C-3	16
C-4	24

2.3 FINITE ELEMENT MODEL

2.3.1 Modeling framework

Timber frame diaphragms consist of multiple components, including studs, rails, sheathing panels, sheathing-to-framing connections, and stud-to-rail connections, all of which must be considered in numerical modeling. The model employed in this study is a 2D mesoscale finite element model developed in MATLAB. It features an interface for defining diaphragm parameters, such as wall height, wall length, sheathing panel length, connector spacing, and the possible presence of center studs. Addi-

https://doi.org/10.52202/080513-0371

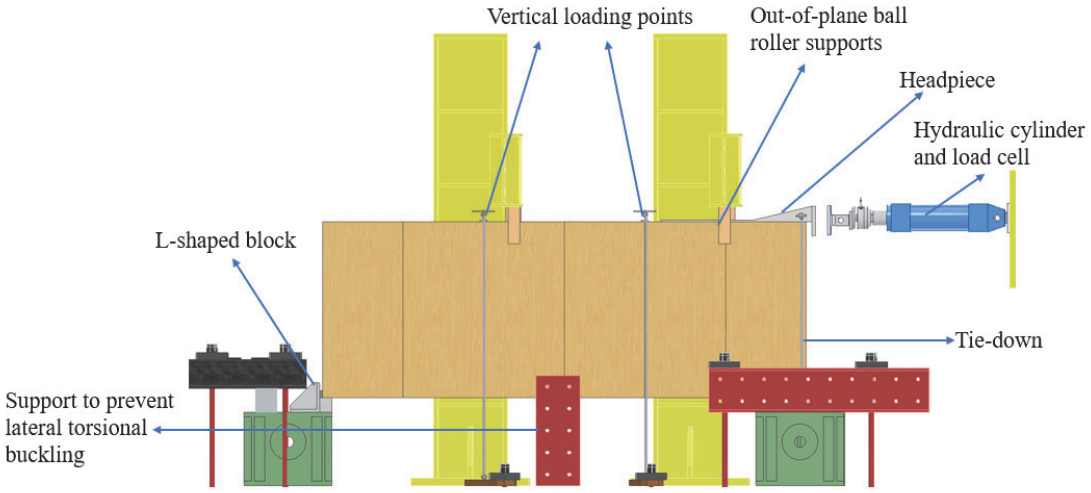

Figure 3: Experimental setup for the shear and combined loading tests.

tionally, imposed forces, displacements, and support conditions can be specified. A generated wall diaphragm is shown in Figure 4.

The second component of the modeling framework is the analysis tool, which performs a materially nonlinear analysis of the wall diaphragm. To ensure computational efficiency, the model employs different element types: plane stress continuum elements for sheathing panels, beam elements for framing components, and nonlinear orthotropic spring elements for sheathing-to-framing connections. In this study, stud-to-rail connections are modeled as hinges or contact elements, preventing deformations at these locations. Consequently, the model's nonlinearity is governed solely by the nonlinear spring elements, which play a critical role in capturing the structural behavior of the timber frame wall.

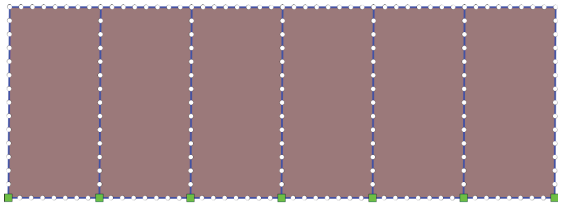

Figure 4: A 2D view of the wall generated by the finite element model. White dots represent the sheathing-to-framing connections, and green squares represent the stud-to-rail connection on the lower rail.

2.3.2 Sheathing-to-framing connections

The sheathing-to-framing connection behavior is governed by a multilinear connection model, which uses damage evolution laws that are calibrated by shear experiments in which the load acts either parallel or perpendicular to the grain of the timber element (rail or stud) [6]. The experimental average of each test is approached through the segmentation by linear lines, further called the multilinear law. This approximation is shown in Figure 5. Both sets of multilinear laws are coupled with each other since

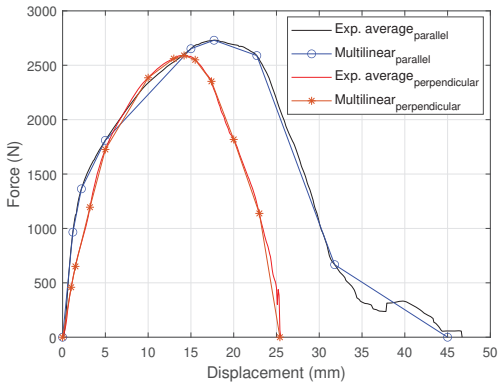

Figure 5: Experimental average and multilinear approximation of the load-displacement diagrams for loading in parallel and perpendicular direction to the timber members.

possible loading in one direction also influences the load-displacement behavior in the opposing direction. The coupling is performed through the use of an interaction ellipse, as discussed in [18], which lowers the load capacity in one direction depending on the amount of displacement or force in the opposite direction by using a projected displacement value. The paired or coupled multilinear laws are further represented by spring elements, which are oriented depending on their initial displacement trajectory, which is defined at time zero during initial loading. The oriented spring pair model is based on [8]. Due to the simple nature of the damage-based modeling approach, which uses a set of scalar damage parameters that reduce the stiffness of a failing sheathing-to-framing connection, the overall stability of the model is excellent while ensuring the model's capabilities to capture the increasing weakening of the connection behavior under increasing loads.

https://doi.org/10.52202/080513-0371

Table 2: Experimental results.

ID	F_{max}(kN)	F_{yield}(kN)	d_{yield}(mm)	$d_{failure}$(mm)	Main failure mode
S-1	93.6	-	-	41	Sheathing tear-out
S-2	101.6	60.2	18	72	Sheathing tear-out
C-1	102.5	57.9	15	65	Sheathing tear-out
C-2	98.5	52.5	14	63	Sheathing tear-out and splitting lower rail
C-3	96.8	52.0	12	52	Sheathing tear-out
C-4	87.5	46.8	11	46	Sheathing tear-out

3 – RESULTS AND DISCUSSION

3.1 EXPERIMENTAL RESULTS

3.1.1 Shear experiments

The shear experiments produced two force-displacement diagrams, serving as references for comparison with the combined shear-bending tests. In the first experiment (Table 2, Figure 6), the peak force reached 93.6 kN, with failure occurring at a horizontal displacement of 41 mm. However, results from the S-I specimen should be interpreted cautiously due to multiple load applications during testing. Initial setup faults required resetting the test before stable conditions were achieved. Consequently, the force-displacement diagram in Figure 6, taken from the final test, shows increased stiffness up to a critical displacement of approximately 15 mm.

The second experiment (S-2) produced a more predictable force-displacement response, reaching a peak force of 101.6 kN, with failure occurring at 72 mm. A minor drop in force at 52 mm was attributed to a temporary slip in the steel tie-down cable, which self-corrected. Without this slip, the peak force may have been slightly higher. Both specimens exhibited a similar failure mechanism, characterized by sheathing-to-framing connection failure at the lower rail and the second-to-last wall stud (Figure 7). The connectors in the lower rail failed first, followed by subsequent failures in the wall stud. The failure occurred as the sheathing panels tore away from the sheathing-to-framing connections while the connections themselves remained intact with the framing. During testing, unevenly distributed "rotation" or racking of the sheathing panels was observed, leading to localized failure.

3.1.2 Combined loading experiments

The combined loading experiments produced distinct force-displacement diagrams (Figure 6), which were used for further analysis. The first specimen, subjected to a vertical load equal to 10% of its maximum vertical load-bearing capacity, exhibited a slight increase in force compared to S-2. However, its horizontal displacement at failure was reduced by 7 mm. Specimen C-2, with a vertical preload of 12 kN, experienced a 4 kN decrease in maximum horizontal force and a 2 mm reduction in displacement at failure compared to C-1. This trend continued for specimens C-3 and C-4, where both the horizontal failure force and displacement at failure progressively decreased with increasing vertical preload.

A second trend was observed in the yielding behavior. According to Section 3.2, S-2 had a yielding force of 60.2 kN at a displacement of 18 mm. Subsequent specimens exhibited a reduction in both yield force and yield displacement, correlating with the level of vertical preloading; a higher preload resulted in earlier yielding.

The dominant failure mode, except for specimen C-2, was sheathing tear-out from the sheathing-to-framing connections. This failure occurred as the OSB detached from the screws while the screws remained connected to the timber frame, as shown in Figure 7. In all cases, failure was localized at the second-to-last stud from the loading side. Specimen C-2 showed a splitting of the lower rail located underneath the second to last stud (Figure 7d). The most likely reason that the splitting occurred at this location was due to a knot located in the timber in this area.

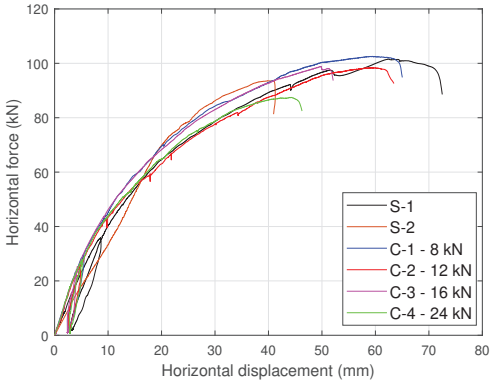

Figure 6: Force-displacement diagrams of the shear and combined loading experiments.

3.2 NUMERICAL RESULTS

3.2.1 Shear resistance

The simulations performed to evaluate the shear resistance, utilizing the FEM framework described in Section 2.3, yielded results that closely matched the experimental data, especially within the elastic and elastoplastic area, as demonstrated in Figure 8. The force displacement response gathered from the numerical model exhibited a strong correlation with the experimental results, indicating the accuracy and reliability of the adopted modeling approach. In particular, the response of specimen S-2 demonstrated a remarkable agreement, with a difference in stiffness of only 2% up to a displacement of 25 mm. Beyond this threshold, the discrepancy gradually increased but remained within an acceptable margin, reaching a peak deviation of approximately 5% until a drop was observed in the

https://doi.org/10.52202/080513-0371

Table 3: Numerical results.

ID	F_{max}(kN)	F_{yield}(kN)	d_{yield}(mm)	$d_{failure}$(mm)	Num./Exp. ratio (F_{max})	Num./Exp. ratio (F_{yield})
S	116.8	70.0	24	87	1.15	1.16
C-1	108.2	69.2	22	71	1.06	1.19
C-2	103.5	65.3	21	61	1.05	1.24
C-3	97.9	63.9	21	54	1.01	1.23
C-4	87.7	58.3	20	49	1.00	1.24

Figure 7: Pictures of the most common failure modes. (a) Failure located in the second-to-last stud; (b) Tearing of OSB; (c) Localized tearing of sheathing in the lower rail; and (d) Splitting underneath the second-to-last stud.

experimental data, as previously discussed. Additionally, the predicted values for both the failure and yielding forces were proportional to the experimental results. Specifically, the numerical model estimated the capacity for both forces to be around 15% higher than the experimentally measured values. These findings suggest that the developed FEM provides a robust and reliable approximation of shear resistance behavior.

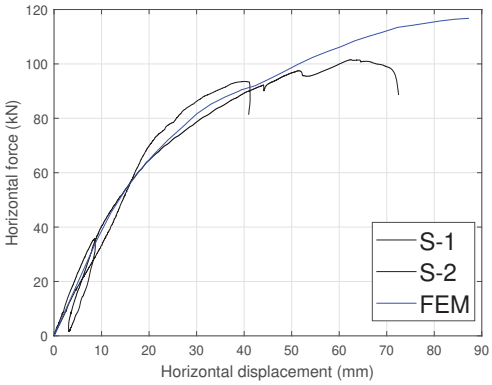

Figure 8: Comparison of the experimental and the finite element model regarding lateral resistance.

3.2.2 Combined loading

The simulations conducted to evaluate the combined loading configurations produced mixed results. The predictions of the finite element model regarding the maximum allowable lateral force demonstrated a high level of accuracy, with deviations remaining within acceptable limits. The highest observed difference was only 6% for configuration C-1. Notably, specimen C-4 yielded particularly accurate results, with a numerical-to-experimental ratio of exactly 1.00, highlighting the model's reliability for this specific case. However, differences between the simulated and experimental outcomes were observed in the initial stiffness values. A comparison of Figures 6 and 9 reveals that, during the experimental campaign, the initial stiffness of the tested specimens exhibited a slight increase. In contrast, the numerical model did not replicate this trend and instead displayed a decrease in initial stiffness as the applied vertical preload increased. This inconsistency suggests that differences in how vertical loading was applied in the experimental setup and the numerical model could have contributed to the observed variations. In the physical tests, vertical preloads were applied using spanners connected to the underlying reaction floors. Conversely, in the numerical model, the applied forces were idealized, acting directly on both studs while remaining aligned with the horizontal movement of the structure, preventing a potential horizontal component due to loading. This idealized application likely contributed to the observed reduction in initial stiffness within the numerical simulations.

The expected decrease in initial stiffness within the numerical model can be attributed to how vertical forces were distributed among the connectors. Specifically, in the simulation, the preload forces were allocated to each connector, potentially initiating damage during the vertical preloading stage before applying horizontal loading. As horizontal forces were subsequently introduced, these pre-existing reductions in stiffness further influenced the overall response, leading to a lower initial stiffness in the global force-displacement behavior. The discrepancy in initial stiffness directly impacts the yielding force predictions, as shown in the numerical results summarized in Table 3. The relatively large variation in yielding forces observed between the experimental and simulated results can be traced back to this initial stiffness difference.

However, despite the observed differences in initial stiffness, the overall trends in both the numerical and experimental configurations remained consistent. In both cases, an increase in vertical preloading resulted in a reduction in the maximum allowable horizontal load and the corresponding displacement at failure. This trend was also visible in the yielding force and yielding displacement, both of which decreased as the vertical preload increased.

https://doi.org/10.52202/080513-0371

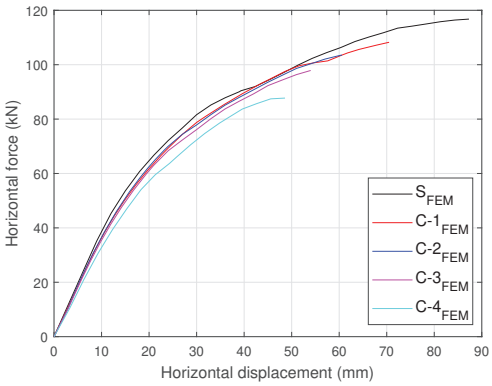

Figure 9: Force-displacement diagram of the FEM simulations of the combined loading configurations.

3.2.3 Prediction of failure location

The finite element model can also be used to predict the failure mode and the specific location where failure is most likely to occur. By simulating the force distribution across the sheathing-to-framing connections, the model provides insights into the load transfer mechanisms within the structure. The numerical analysis enables the visualization of these forces for each connector element, offering a relative representation of their magnitude and direction. While the displayed forces are not absolute, they serve as valuable indicators of potential failure locations.

Figure 10 illustrates two distinct stages of the loading process, each with its corresponding force distribution. The left diaphragm represents the state of the diaphragm at the initial time step when lateral loading is first applied (after vertical preload). As shown, the force distribution on the opposite side of the applied loading increases, while the forces on the same side as the applied load decrease. This behavior reflects the expected redistribution of internal forces as the structure responds to the external loading. The right diaphragm in Figure 10 captures the state of the diaphragm at a crucial moment just before total failure occurs. At this stage, the forces on the side opposite to the applied loading experience significant amplification (superposition effect), suggesting that failure is most likely to initiate in this region. Figure 11 shows how the model predicts this in a 2D view. This numerical prediction aligns with physical observations from the experimental campaign, reinforcing the model's capability to estimate failure locations based on force distribution patterns.

4 – CONCLUSION

This research examined the structural behavior of timber frame diaphragms under combined bending and shear loading through experimental testing and numerical modeling. The findings indicate that increased vertical loading reduces the horizontal racking resistance, as evidenced by decreased yielding force, yielding displacement, and stiffness.

The experimental results revealed that the primary failure mode across all specimens was sheathing tear-out at the sheathing-to-framing connections, particularly near the second-to-last stud from the loading side. In one case, additional splitting of the lower rail was observed, likely influenced by timber knots at this location. The observed failure behavior suggests that increasing vertical load amplifies stress concentrations at critical connection points, accelerating failure initiation.

The used FEM framework accurately predicted force-displacement behavior and failure locations, with deviations in peak force remaining within an acceptable range. However, discrepancies in initial stiffness suggest that further refinement of the numerical modeling approach, particularly in the application of vertical preloads, may enhance predictive accuracy. Despite these differences, the model accurately captured the general trends observed in experimental results, reinforcing its applicability for assessing timber frame diaphragm performance under combined loading conditions.

These findings underscore the importance of considering combined loading effects in the design of timber structures, particularly in scenarios where load redistribution may influence failure mechanisms. Future research should focus on full-scale validation, alternative connection configurations, and further refinement of numerical methods to enhance the predictive reliability of timber frame diaphragm behavior under complex loading conditions.

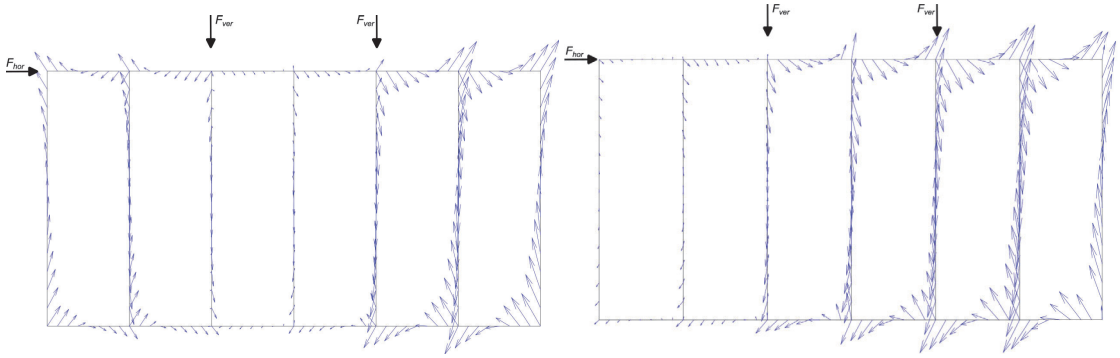

Figure 10: Distribution of sheathing-to-framing connection forces as predicted by the finite element model: (left) Initial time step when lateral loading is added; (right) Time step before failure of the configuration.

https://doi.org/10.52202/080513-0371

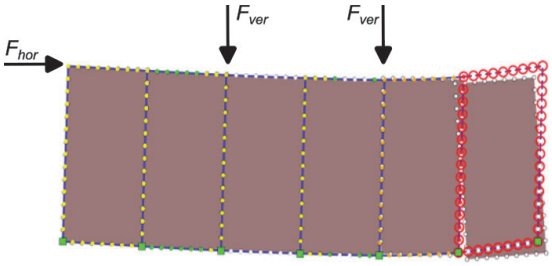

Figure 11: A 2D view of the estimated failure location by the finite element model.

5 – ACKNOWLEDGMENT

The authors gratefully thank the Special Research Fund (BOF) of Hasselt University for supporting this research. BOF reference: BOF22OWB18.

REFERENCES

[1] J. M. Branco and L. A. Neves. "Robustness of timber structures in seismic areas." In: *Engineering Structures* 33 (11 2011), pp. 3099–3105. ISSN: 01410296. DOI: 10.1016/j.engstruct.2011.02.026.

[2] D. Byloos and B. Vandoren. "Experimental and analytical assessment of the racking behavior of timber frame walls with single-sided double-layered sheathing panels." In: *Engineering Structures* 316 (2024). ISSN: 18737323. DOI: 10.1016/j.engstruct.2024.118592.

[3] N. Elkady, L. A. Nelson, L. Weekes, N. Makoond, and M. Buitrago. "Progressive collapse Past, present, future and beyond." In: *Structures* (2024).

[4] European Committee for Standardization. *CEN Enquiry draft prEN 1995-1-1:2023, Eurocode 5 - Design of timber structures - Part 1-1: General rules and rules for buildings*. 2023.

[5] European Committee for Standardization. *EN-1995-1-1: Eurocode 5: Design of timber structures - Part 1-1: General - Common rules and rules for buildings*. 2005.

[6] European Committee for Standardization. *NBN-EN-1381: Tests methods Load Bearing Load bearing nails, screws, dowels and bolts*. 2009.

[7] J. A. Huber, M. Ekevad, U. A. Girhammar, and S. Berg. "Structural robustness and timber buildings–a review." In: *Wood Material Science and Engineering* 14 (2 2019), pp. 107–128. ISSN: 17480280. DOI: 10.1080/17480272.2018.1446052.

[8] J. P. Judd and F. S. Fonseca. "Analytical Model for Sheathing-to-Framing Connections in Wood Shear Walls and Diaphragms." In: *Journal of Structural Engineering* 131 (2 2005), pp. 345–352. ISSN: 0733-9445. DOI: 10.1061/(asce)0733-9445(2005)131:2(345).

[9] F. Kiakojouri, V. D. Biagi, B. Chiaia, and M. R. Sheidaii. "Progressive collapse of framed building structures: Current knowledge and future prospects." In: *Engineering Structures* 206 (2020). ISSN: 18737323. DOI: 10.1016/j.engstruct.2019.110061.

[10] L. Kuai, S. Ormarsson, and J. Vessby. "Nonlinear FE-analysis and testing of light-frame timber shear walls subjected to cyclic loading." In: *Construction and Building Materials* 362 (2023). ISSN: 09500618. DOI: 10.1016/j.conbuildmat.2022.129646.

[11] T. Malmqvist, M. Nehasilova, A. Moncaster, H. Birgisdottir, F. N. Rasmussen, A. H. Wiberg, and J. Potting. "Design and construction strategies for reducing embodied impacts from buildings – Case study analysis." In: *Energy and Buildings* 166 (2018), pp. 35–47. ISSN: 03787788. DOI: 10.1016/j.enbuild.2018.01.033.

[12] K. Pintarič and M. Premrov. "Mathematical modelling of timber-framed walls using fictive diagonal elements." In: *Applied Mathematical Modelling* 37 (16-17 2013), pp. 8051–8059. ISSN: 0307904X. DOI: 10.1016/j.apm.2013.02.050.

[13] J. D. Sørensen. "Framework for robustness assessment of timber structures." In: *Engineering Structures* 33 (11 2011), pp. 3087–3092. ISSN: 01410296. DOI: 10.1016/j.engstruct.2011.02.025.

[14] A. Teischinger. "Opportunities and limits of timber in construction." In: *Proceedings of the World Conference on Timber Engineering (WCTE 2016)* (2016). URL: https://www.researchgate.net/publication/307174358.

[15] A. Togay, Ö. Anil, Ü. K. Işleyen, İ. Ediz, and C. Durucan. "Finite-element analyses of light timber-framed walls with and without openings." In: *Proceedings of the Institution of Civil Engineers: Structures and Buildings* 170 (8 2017), pp. 555–569. ISSN: 17517702. DOI: 10.1680/jstbu.16.00085.

[16] L. Tupenaite, L. Kanapeckiene, J. Naimaviciene, A. Kaklauskas, and T. Gecys. "Timber Construction as a Solution to Climate Change: A Systematic Literature Review." In: *Buildings* 13 (4 2023). ISSN: 20755309. DOI: 10.3390/buildings13040976.

[17] F. Véliz, M. F. Chacón, J. Lagos, S. Berwart, N. López, and P. Guindos. "Structural performance of strong timber diaphragms: High-capacity light-timber frames and cross-laminated timber." In: *Structures* 63 (2024). ISSN: 23520124. DOI: 10.1016/j.istruc.2024.106335.

[18] J. Vessby, E. Serrano, and A. Olsson. "Coupled and uncoupled nonlinear elastic finite element models for monotonically loaded sheathing-to-framing joints in timber based shear walls." In: *Engineering Structures* 32 (11 2010), pp. 3433–3442. ISSN: 01410296. DOI: 10.1016/j.engstruct.2010.05.018.

https://doi.org/10.52202/080513-0371

[19] K. Vogrinec, M. Premrov, and E. K. Šilih. "Simplified modelling of timber-framed walls under lateral loads." In: *Engineering Structures* 111 (2016), pp. 275–284. ISSN: 18737323. DOI: 10.1016/j.engstruct.2015.12.029.

[20] K. Voulpiotis, J. Köhler, R. Jockwer, and A. Frangi. "A holistic framework for designing for structural robustness in tall timber buildings." In: *Engineering Structures* 227 (2021). ISSN: 18737323. DOI: 10.1016/j.engstruct.2020.111432.

[21] K. Voulpiotis, S. Schär, and A. Frangi. "Quantifying robustness in tall timber buildings: A case study." In: *Engineering Structures* 265 (2022). ISSN: 18737323. DOI: 10.1016/j.engstruct.2022.114427.